energy&fuels

Article

pubs.acs.org/EF

Effect of Reaction Temperature on the Chemical Looping Combustion of Coal with $CuFe_2O_4$ Combined Oxygen Carrier

Baowen Wang,*[,†,‡] Qiang Ma,[†] Weishu Wang,[†] Chuan Zhang,[†] Daofeng Mei,[§] Haibo Zhao,[‡] and Chuguang Zheng[‡]

[†]College of Electric Power, North China University of Water Resources and Electric Power, Zhengzhou 450045, China

[‡]State Key Laboratory of Coal Combustion, Huazhong University of Science and Technology, Wuhan 430074, China

[§]College of Engineering, Huazhong Agricultural University, Wuhan 430070,China

ABSTRACT: Reaction temperature is regarded as one of the important factors influencing the efficient utilization of coal in chemical looping combustion (CLC), but research into its effect on the chemical structure of coal in CLC is limited. In the research reported herein, the oxygen-transfer mechanism of $CuFe_2O_4$ prepared through the sol−gel method combined with combustion synthesis, along with the characteristics of its reaction with a typical coal of high sulfur and high ash contents (abbreviated as LZ), were systematically investigated at different final reaction temperatures, with the research focused on the effect of reaction temperature. H_2-temperature-programmed reduction of $CuFe_2O_4$ indicated that the first reduction of the Cu^{2+} ion in $CuFe_2O_4$ was advantageous in the later transmission of atomic oxygen from the Fe^{3+} reduction, while temperature-programmed decomposition of $CuFe_2O_4$ under a N_2 atmosphere validated the potential of $CuFe_2O_4$ to emit O_2 through its direct decomposition. Furthermore, thermogravimetric analysis and Fourier transform infrared spectroscopy showed better reaction performance between $CuFe_2O_4$ and LZ coal than other ferrite oxygen carrier (OC) candidates, such as $MnFe_2O_4$, $NiFe_2O_4$, and $CoFe_2O_4$, which we studied previously. Comprehensive characterization of the solid products from reaction of $CuFe_2O_4$ with LZ coal by field emission scanning electron microscopy coupled with energy-dispersive X-ray spectroscopy, X-ray diffraction, and X-ray photoelectron spectroscopy (XPS) indicated that $CuFe_2O_4$ was mainly reduced to Cu and Fe_3O_4. At the same time, some oxygen-deficient $CuFe_2O_4$ was also formed through disintegration of the original $CuFe_2O_4$ spinel with more Cu^{2+} and Fe^{3+} ions occupying the octahedral sites, which benefited the transmission of the atomic oxygen involved in the $CuFe_2O_4$. Finally, XPS analysis of the LZ coal residue after its reaction with $CuFe_2O_4$ indicated that the main obstacle to fully utilizing LZ coal at the molecular scale in CLC was the dominance of C−C/C−H groups, with the highest relative content over 62% at the 700 °C reaction temperature. Increasing the reaction temperature was quite effective to promote the efficient utilization of LZ coal from the molecular perspective during the reaction between LZ coal and $CuFe_2O_4$.

1. INTRODUCTION

Fossil fuels, especially coal, are the dominant primary energy sources now and in the foreseeable future to satisfy the expanding energy demand, because of their relative abundance and easy accessibility. Especially in China, the high dependence on coal for energy brings about serious environmental impacts, such as gas pollution, global warming, and greenhouse gas effect, which have aroused great public concern.[1] Therefore, it is greatly worthwhile to explore novel coal combustion technologies for efficient conversion of coal as well as simultaneous cost-effective control of pollution emission. Among various coal combustion technologies, chemical looping combustion (CLC) has gained much interest for its prominent merits, including capture of CO_2 without great energy penalty,[2] efficient inhibition of NO_x formation,[3] and energy cascade utilization,[4] where an active oxygen carrier (OC) is adopted to substitute air and transmitted multiple cycles in real CLC systems consisting of a fuel reactor (FR) and an air reactor (AR) so as to realize both coal oxidization and regeneration of the reduced OC for the ensuing continuous operation of CLC.

To date, directly fuelled coal CLC has been intensively investigated, and the slow gasification rate of coal is ascertained as the limiting step for efficient conversion of coal.[2,5,6] In order to increase utilization of coal in CLC and avoid detrimental effects of the unburnt noncondensable gases (such as combustible H_2, CO, and CH_4) on the capture of CO_2 in the downstream flue gas, various measures have been attempted, such as use of combined OCs[7,8] or modified OCs,[9−11] increase of the reaction temperature[12,13] and system pressure,[14,15] enhancement of the mass ratio of OC to coal,[16,17] adoption of extra technological options[18] (e.g., flue gas recycling or carbon stripper addition), and application of chemical looping with oxygen uncoupling (CLOU) as an alternative solution.[19] Overall, among all the measures listed, varying the reaction temperature is regarded as one of the preferential measures to promote coal utlization, as frequently investigated in the CLC process.

The chemical structure of coal has a strong influence on its reactivity.[20] Deep insight into coal's chemical structure and the transformations it undergoes is significant for efficient utilization of coal.[21,22] So far, many studies have been focused on changes in coal's chemical structure during various processes related to its thermal conversion, e.g., coal pyrolysis[23] and gasification,[24] low-temperature oxidation,[25] and combustion.[26]

Received: October 1, 2016
Revised: March 21, 2017
Published: April 19, 2017

DOI: 10.1021/acs.energyfuels.6b02525
Energy Fuels 2017, 31, 5233−5245

Table 1. Textural Characteristics and Crystalline Structure of the Prepared $CuFe_2O_4$

		single-point absorption		main species	
sample	BET surface area (m^2/g)	total pore volume (cm^3/g)	average pore size (nm)	crystalline structure	crystalline size (nm)
CuO[a]	0.5920[a]	0.000468[a]	15.9448[a]	monoclinic	107.3[a]
$CuFe_2O_4$	0.6448	0.001082	9.7013	tetragonal	56.6
Fe_2O_3	0.6823	0.001390	9.3567	rhombohedral	89.2[a]

[a]As reported in our previous research.[31]

But transformation of the chemical structure of coal in CLC with introduction of an OC is quite complex and has not been fully studied because of the competing reactions involved in coal pyrolysis, residual char gasification and oxygen transfer from OC. Thus, though direct characterization of the changing chemical structure of coal is a great challenge, the evolution of coal's chemical structure involved in CLC can be investigated to gain a more in-depth understanding about coal from the molecular perspective, to promote its efficient conversion.

In our previous research,[7,8,27,28] the reaction of coal with a $CuFe_2O_4$ combined OC was evaluated, and $CuFe_2O_4$ was verified as a promising OC with such advantages as superior reactivity over its single reference oxides CuO and Fe_2O_3, good resistance to sintering, wide fuel adaptability to coal of different ranks, and great potential to realize simultaneous CO_2 capture and in situ desulfurization. Meanwhile, the influence of an excess number of $CuFe_2O_4$ OCs on the variation of the coal chemical structure was also investigated in our previous research.[29] Along with the excess OC, the reaction temperature is considered to be another important influencing factor. Therefore, in this research, the influence of reaction temperature on $CuFe_2O_4$ oxygen transfer and the evolution of coal's chemical structure was further investigated. The mechanisms involved in oxygen transfer of the prepared $CuFe_2O_4$—both atomic oxygen transfer and gaseous O_2 emission—were studied using temperature-programmed reduction (TPR) with H_2 as the model fuel and temperature-programmed decomposition (TPD) under a N_2 atmosphere, respectively. The characteristics of the reaction between the prepared $CuFe_2O_4$ OC and a typical Chinese bituminous coal of high sulfur and high ash contents (abbreviated as LZ) was investigated via thermogravimetric analysis (TGA) and Fourier transform infrared (FTIR) spectroscopy at different final temperatures from 700 to 1000 °C. The solid reaction products between LZ coal and $CuFe_2O_4$ were carefully collected and further studied through field emission scanning electron microscopy (FESEM) coupled with both energy-dispersive X-ray spectroscopy (EDX) and X-ray diffraction (XRD) analysis. The chemical structure of coal and its evolution during the reaction of coal with $CuFe_2O_4$ at the different final temperatures were also characterized using X-ray photoelectron spectroscopy (XPS) so as to enhance the understanding of coal's chemical structure at the molecular level for improved utilization of coal in CLC.

2. EXPERIMENTAL PROCEDURES

2.1. Materials Preparation and Characterization. The $CuFe_2O_4$ OC, with two active oxide components such as CuO and Fe_2O_3, was synthesized using a sol−gel technique combined with combustion synthesis (SGCS), developed previously in our group,[30] with urea, hydrated nitrates of copper, and iron as the precursors. As validated in our previous research,[7,27] the prepared $CuFe_2O_4$ shows good performance, including good reactivity and high resistance to sintering over multiple cycles. After sequential procedures of gel preparation and ignition, the as-prepared $CuFe_2O_4$ was further processed at 950 °C for 2 h in a muffle furnace under an air atmosphere.

After the OC was prepared, it was ground and sieved, with particles between 63 and 106 μm collected and further characterized as shown in Table 1, where phases involved in the prepared OCs and their crystalline structures were studied by step-scanning using X'Pert PRO XRD (PANalytical Corp., Netherlands) with Cu Kα radiation at 40 kV and 40 mA over 10−90°. The textural structural characteristics of the prepared OCs, including the Brunauer−Emmett−Teller (BET) specific surface area, pore volume, and pore size distribution, were evaluated using a Micrometrics physical adsorption analyzer (ASAP 2020, USA).

The coal sample originated from LiuZhi of Guizhou province and is herein designated as LZ. After drying and crushing, the LZ coal was further sieved, with particles between 63 and 106 μm collected for later use. Its properties, including proximate, ultimate analysis data and ash components in oxide format, were determined in our previous research on LZ coal.[29] The LZ coal used in this research is a typical Chinese coal with total ash and sulfur contents up to 41.88 and 5.23 wt%, respectively. The major mineral components were inferred to be Si-, Al-, and Fe-based, with their total content higher than 80 wt%.

After separate preparation of $CuFe_2O_4$ OC and the LZ coal sample as described above, based on the LZ coal's properties,[29] 1 kg of LZ coal was determined as $C_{19.9}H_{9.9}N_{0.35}S_{0.95}O_{2.97}$, without the minerals involved. Then, based on mass balance,[7,8] assuming that LZ coal was stoichiometrically oxidized to CO_2, H_2O, and SO_2, and that $CuFe_2O_4$ was fully reduced to Cu and Fe_3O_4, the $CuFe_2O_4$ excess oxygen number Φ was taken as 1. The mass ratio of $CuFe_2O_4$ to LZ coal at Φ = 1 corresponded to 7.84. As to the oxide components CuO and Fe_2O_3, their mass ratios to LZ coal at Φ = 1 were calculated as 3.47 and 20.93, respectively.

The mixture of LZ coal with $CuFe_2O_4$ at the mass ratio determined above was well stirred in a laboratory mortar until they were mixed evenly for use.

2.2. Experimental Methods. $CuFe_2O_4$ combined OC has a complex crystalline structure, and its oxygen-transfer mechanisms are thus complicated—either direct transfer of the atomic oxygen involved or emission of gaseous O_2 through its direct decomposition. In order to illuminate the oxygen-transfer pathways of the SGCS-made $CuFe_2O_4$ well, both H_2-TPR and TPD of the prepared OC under a pure N_2 atmosphere were carried out using an STA 409C simultaneous thermal analyzer (Netzsch Corp., Germany). On one hand, to investigate the reducibility of the prepared $CuFe_2O_4$ via atomic oxygen transfer, about 30 mg of the prepared OC was introduced to the TGA sample pan and heated from the ambient to 800 °C at 25 °C/min in a H_2 stream (20 vol% H_2 in N_2), at a flow rate 80 mL/min. On the other hand, to investigate the emission of gaseous O_2 through direct decomposition of the prepared $CuFe_2O_4$ OC, ∼30 mg of the prepared $CuFe_2O_4$ was heated from the ambient to 950 °C at 25 °C/min under the pure N_2 atmosphere, with the N_2 flow rate set as 80 mL/min. The two oxides, CuO and Fe_2O_3, were also included for reference.

The reaction performance of LZ coal and the synthetic $CuFe_2O_4$ OC was tested in the same STA 409C analyzer. Approximate 15 mg of the mixture of LZ coal and $CuFe_2O_4$ at Φ = 1 was put in the sample pan and heated at 25 °C/min from the ambient to the prescribed final temperatures of 700, 800, 900, and 1000 °C, which covered the realistic CLC reaction temperature range of interest. The duration spent at the final temperature was 10 min, to ensure coal conversion. High-purity N_2 was taken as the carrier gas, and the ideal 80 mL/min

DOI: 10.1021/acs.energyfuels.6b02525
Energy Fuels 2017, 31, 5233−5245

flow rate was determined through several pre-tests that involved changing the flow rate so as to avoid the possible heat- and mass-transfer limitations and to ensure the reaction was mainly initiated under reaction-controlled conditions, and also in this way to make the experimental results reproducible. A parallel TGA experiment for pyrolysis of only LZ coal without addition of $CuFe_2O_4$ was conducted using the similar experimental protocol for reference.

2.3. Conversion of $CuFe_2O_4$ OC with LZ Coal. Reaction of the $CuFe_2O_4$ OC with LZ coal is very complicated and involves different chemical reactions, including pyrolysis/gasification of coal, oxygen transfer from the $CuFe_2O_4$ OC, and their interaction. In order to quantitatively evaluate the oxygen transfer from the $CuFe_2O_4$ OC and its effect on LZ coal, two quantitative conversion indexes developed in our previous research[7,31] were introduced in this research.

First, to quantitatively evaluate the total reaction of LZ coal with $CuFe_2O_4$, the total mixture conversion index $X_{LZ\text{-}OC}$ (%) was defined as shown in eqs 1 and 2,

$$X_{LZ\text{-}OC}(t) = \frac{W_{LZ\text{-}OC}(t=0) - W_{LZ\text{-}OC}(t)}{x_1\Delta W_{OC} + x_2\Delta W_{LZ}} \quad (1)$$

$$f = x_1/x_2 \quad (2)$$

where $X_{LZ\text{-}OC}$ is the total conversion index for the reaction of LZ coal and $CuFe_2O_4$ together (%), $W_{LZ\text{-}OC}$ refers to the fraction of weight losses (wt%), $t = 0$ and t refer to the beginning of the reaction between LZ coal and OC and at the specfic time t, x_1 and x_2 are the weight portions of $CuFe_2O_4$ and LZ coal in the solid mixture (%), f is the ratio of x_1 and x_2 as depicted in eq 2, and ΔW_{OC} and ΔW_{LZ} are the maximum losses for $CuFe_2O_4$ and the LZ coal.

Then, in order to evaluate the oxygen transferred from the OC upon its mixing with LZ coal and its further contribution to the LZ coal conversion, based on the global weight balance throughout the reaction process of LZ coal with OC, the conversion index of OC, i.e., X_{OC}, was defined as shown in eqs 3 and 4,

$$W_{LZ\text{-}OC}(t) = x_1W_{OC}(t) + x_2W_{LZ}(t) \quad (3)$$

$$X_{OC} = \frac{W_{LZ\text{-}OC}(t) - x_2W_{LZ}(t)}{x_1\Delta W_{OC}} \quad (4)$$

where $W_{LZ}(t)$, $W_{OC}(t)$, and $W_{LZ\text{-}OC}(t)$ refer to the weight losses of respectively the LZ coal, $CuFe_2O_4$ OC, and their total mixture occurring at time t (wt%), from which the instantaneous value for $W_{LZ}(t)$ was obtained from the parallel reference experiment using only LZ coal pyrolysis under the same reaction condition. The other variables in eqs 3 and 4 are the same as those defined in eqs 1 and 2 above.

2.4. Comprehensive Investigation of the Reaction Products between LZ Coal and $CuFe_2O_4$. The gaseous products emitted during the TGA from LZ coal reaction with $CuFe_2O_4$ were continuously monitored in situ via FTIR analysis (EQUINOX 55, Bruker Corp., Germany). The IR wavenumber scanning range was 4000−500 cm^{-1}. The sensitivity and resolution of the FTIR were preset at 1 and 4 cm^{-1} prior to the analysis, respectively. Meanwhile, the transfer line between the TGA and the FTIR was heated to 180 °C to eliminate the possibility of tar and steam condensation.

The microscale morphology and elementary distribution of interest for the solid products between LZ coal and $CuFe_2O_4$ were characterized using a Siron 200 field emission scanning electron microscope (FEI Company, The Netherlands) coupled with a Genesis energy-dispersive X-ray spectroscopy instrument (Edax, US) at a magnification of ×5000 and the accumulated voltage of 20 kV. The solid crystallines formed from reaction of LZ coal with $CuFe_2O_4$ were subsequently determined by X-ray diffraction analysis using an X'Pert PRO instrument (PANalytical Corp., Netherlands), which was operated via Cu Kα radiation at 40 mA and 40 kV over 10−90° by step-scanning.

The variation of the chemical states and compositions on the solid products' surface for reaction of LZ coal with $CuFe_2O_4$ at different final temperatures from 700 to 1000 °C was analyzed using a VG MultiLab 2000 X-ray photoelectron spectrometer (Thermo Electron Corp., USA), which was equipped with a monochromatic Mg Kα ($h\nu$ = 1253.6 eV) excitation source and operated at 300 W in the narrow-scanning mode. The pass energy and the base pressure of the XPS were stabilized around 25 eV and 5×10^{-8} Pa to ensure good sensitivity. For all of the scanned elements, their binding energies were calibrated relative to the reference C 1s peak at 284.6 eV. The obtained XPS scanning data for the species studied were then curve-fitted according to the mixed Gaussian−Lorentzian functions. The relative atomic concentration of the chemical species of interest was quantified according to the fitted XPS peak areas.

3. RESULTS AND DISCUSSION

3.1. Oxygen-Transfer Mechanisms for $CuFe_2O_4$ OC. Both the crystalline and structural characteristics of OC are important for its oxygen transfer. Therefore, the phase compositions of the SGCS-prepared $CuFe_2O_4$ and its two reference oxides, CuO and Fe_2O_3, were identified using XRD and are shown in Figure 1. From the XRD patterns presented

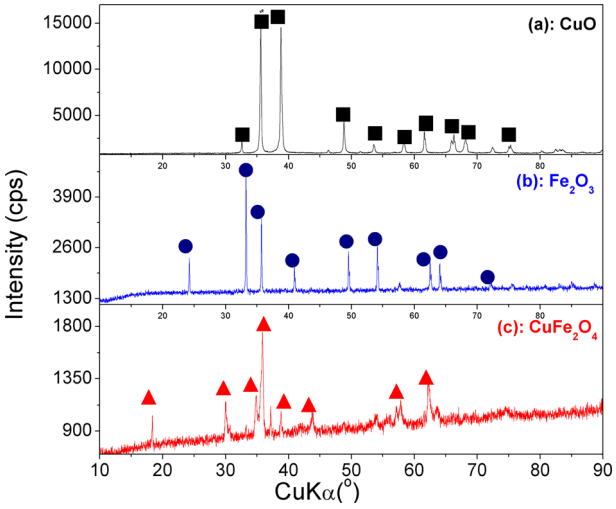

Figure 1. XRD patterns of the prepared $CuFe_2O_4$ and its single oxides CuO and Fe_2O_3.

in Figure 1, separate phases CuO, α-Fe_2O_3, and $CuFe_2O_4$ are identified on the basis of well-defined XRD peaks. During 2 h of processing at 950 °C under the air atmosphere, the grain sizes of the prepared $CuFe_2O_4$ and its oxides were calculated by using the Scherrer equation, $D = 0.9\lambda/(\beta \cos \theta)$, where D refers to the crystalline size (nm), λ is the Cu Kα radiation wavelength (λ = 0.15406 nm), θ represents the radian diffraction angle, and β is the corrected half-width for instrument broadening. Next, the grain size of the prepared CuO was calculated as 107.3 nm, much higher than that of the prepared Fe_2O_3 (89.2 nm), mainly due to the inferior resistance to sintering of CuO compared to Fe_2O_3. However, the measured grain size of the prepared $CuFe_2O_4$ is only 56.6 nm, much lower than those of both CuO and Fe_2O_3 due to the tetragonal crystalline structure of the prepared $CuFe_2O_4$, which is different from the monoclinic and rhombohedral ones of CuO and Fe_2O_3, respectively. In contrast, in terms of the textural characteristics of the prepared $CuFe_2O_4$, as shown in Table 1, the BET surface area, the pore volume, and the average pore size of the prepared $CuFe_2O_4$ OC fell close to the values of CuO and Fe_2O_3.

Furthermore, in order to investigate the reducibility of the prepared $CuFe_2O_4$ OC, H_2-TPR was conducted, with the

DOI: 10.1021/acs.energyfuels.6b02525
Energy Fuels 2017, 31, 5233−5245

reduction results shown in Figure 2a. It was found that CuO began to lose atomic oxygen at 170 °C, ending at around 235

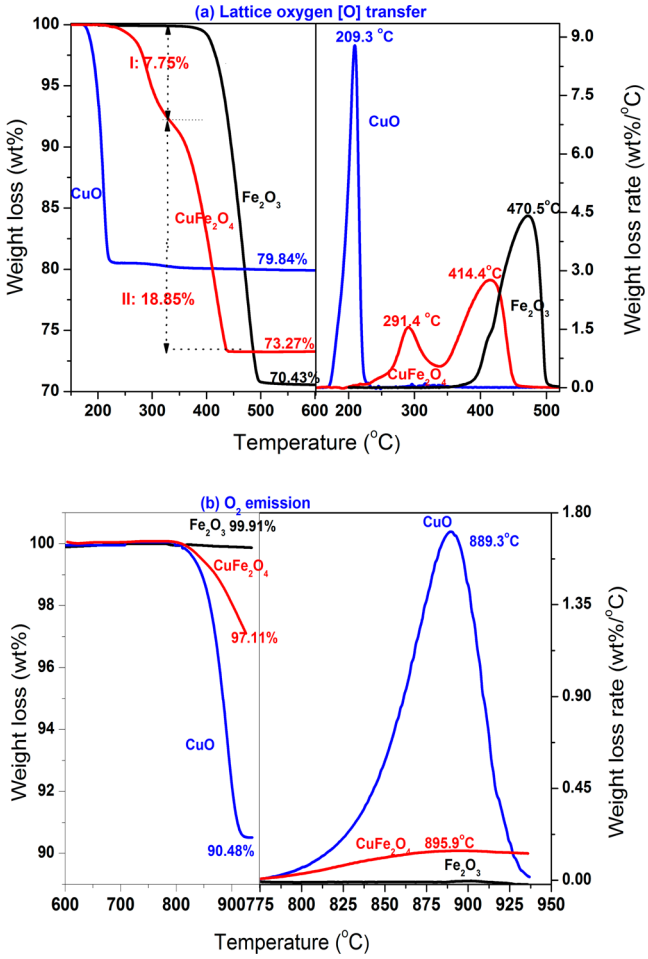

Figure 2. $CuFe_2O_4$ oxygen-transfer mechanisms. (a) Atomic oxygen [O] transfer through temperature-programmed reduction (TPR) of the $CuFe_2O_4$ with model fuel H_2. (b) O_2 emission through temperature-programmed decomposition (TPD) of the $CuFe_2O_4$ under N_2 atmosphere.

°C, with the final weight loss reaching 79.84%, meaning that CuO reached its theoretical oxygen capacity of ~21% (= (16 × 100)/79.55), with nearly all the atomic oxygen transferred to the H_2. During TPR of CuO, only one reduction reaction stage of CuO with H_2 was identified, and the maximal weight loss rate reached 8.79 wt%/°C at a peak temperature around 209.3 °C. For Fe_2O_3, both the starting and the end temperatures were higher than those of CuO, reaching 373.5 and 502.9 °C, respectively. Meanwhile, the Fe_2O_3 maximal reduction rate of weight loss was 4.41 wt%/°C at the temperature of 470.5 °C, much lower than that of CuO, which fully verified the lower reactivity of Fe_2O_3 than that of CuO.

But far different from these two reference oxides above, two squential reaction stages were observed for $CuFe_2O_4$ reduction with H_2. Its first reaction stage commenced at 220.1 °C, with 7.75% of the atomic oxygen lost. Based on the weight fraction of one atomic oxygen in the $CuFe_2O_4$ equal to 6.7% (= (16 × 100)/239.24), more than one equivalent atomic oxygen was transferred from the $CuFe_2O_4$ at the first reaction stage and the elemental Cu was formed, similar to the findings of Shin and Choi.[32] Furthermore, at the second reaction stage, another 18.85% of the oxygen was lost, which meant more than two equivalent atomic oxygens were transferred, as accompanied by the reduction of the Fe^{3+} ion involved in the $CuFe_2O_4$. Meanwhile, the maximal reduction rate of $CuFe_2O_4$ weight loss at the secondary reduction stage was 2.76 wt%/°C, nearly two times of that reduction rate of the Cu^{2+} ion at the first reaction stage, which is just on the contrarry to the observed maximal weight loss rate of CuO reduction with H_2 higher than that of Fe_2O_3 as observed above, which implied that the initial reduction of the Cu^{2+} greatly improved the reactivity of Fe^{3+} and also promoted the faster transfer of the atomic oxygen involved in the $CuFe_2O_4$. Therefore, the end temperature for $CuFe_2O_4$ reduction by H_2 is much lower (454.6 °C) than that of the reference Fe_2O_3 (502.9 °C), and thus the beneficial reaction synergistic effect of $CuFe_2O_4$ over the two reference oxide CuO and Fe_2O_3 was created, as found in our previous research,[7,27] though the fuels used were different. Finally, the final weight loss of $CuFe_2O_4$ after H_2 reduction reached 73.27% and approached its maximal theoretical oxygen capacity of $CuFe_2O_4$ (26.7%) by transferring all the atomic oxygens involved through the pathway $CuFe_2O_4 \rightarrow Cu + 2Fe + 4[O]$.

To study the O_2 emission behavior, $CuFe_2O_4$ and their two reference oxides were investigated using the TPD experiment under the pure N_2 atmosphere and shown in Figure 2b. It could be found that CuO easily decomposed to emit O_2 through the pathway $2CuO \rightarrow 2Cu_2O + O_2$ with the maximal weight loss rate reaching 1.71 wt%/°C at the peak temperature 889.3 °C. From the starting temperature 780.6 °C to the end temperature 938.9 °C, the CuO was almost completely decomposed with the final weight loss stabilized at 90.48%, similar to the finding from Hosseini et al.[33] Meanwhile, its inferior resistance to sintering and potential to agglomeration and defluidization for CuO could be overcome by the upgraded production method with relevant inert support introduced.[34] While for Fe_2O_3, it was inert below 1000 °C with nearly indiscernible decomposition. As for $CuFe_2O_4$, it began to decompose at the starting temperature 810.5 °C, lower than the reported decomposition temperature as 839 °C for the $CuFe_2O_4$ prepared using the coprecipitation method,[35] which meant the higher decomposition reactivity of the SGCS-made $CuFe_2O_4$ in this research. As the decomposition temperature increased, $CuFe_2O_4$ decomposition rate was also improved with the maximal weight loss rate reaching 0.1444 wt%/°C at the peak temperature 895.9 °C. But further increase in the decomposition temperature up to 950 °C, complete decomposition of the $CuFe_2O_4$ was not reached, which agreed with the finding of Yu et al.[36] The final weight loss of $CuFe_2O_4$ reached 97.11% by emission of the O_2 through direct decomposition of the $CuFe_2O_4$ to $CuFeO_2$ and Fe_2O_3 ($4CuFe_2O_4 \rightarrow 4CuFeO_2 + 2Fe_2O_3 + O_2$).[7,37] The O_2 emission capacity of $CuFe_2O_4$ attained 0.0289 g/(g $CuFe_2O_4$), which is larger than that of the most promising $CaMnO_{3-\delta}$ OC with the O_2 emission capacity reported as 0.0252 g O_2/g OC[38] and thus applicable to the realistic CLC system with great potential.

Overall, the preliminary investigation on the oxygen-transfer mechanism of the SGCS-$CuFe_2O_4$ above fully revealed the beneficial reaction synergism of the $CuFe_2O_4$ through the first reduction of the Cu^{2+} ion in the $CuFe_2O_4$ during its TPR process and the O_2 emission capacity of $CuFe_2O_4$ through its direct decomposition during the TPD process. Such a flexible oxygen-transfer mechanism of $CuFe_2O_4$ would be desired in a realistic directly fueled coal CLC system.

DOI: 10.1021/acs.energyfuels.6b02525
Energy Fuels 2017, 31, 5233−5245

3.2. Reaction Behavior of LZ Coal with $CuFe_2O_4$ OC by TGA. According to the oxygen-transfer mechanisms of $CuFe_2O_4$ OC studied above, the characteristics for the reaction of LZ coal and the $CuFe_2O_4$ OC at $\Phi = 1$ in the pure N_2 stream were further evaluated in the same TGA apparatus. Four different final temperatures were considered: 700, 800, 900, and 1000 °C. Profiles of the final weight loss (TG) and its weight loss rate (DTG) over time for the LZ coal reaction with $CuFe_2O_4$ OC at the different final temperatures are given in Figure 3. At the same time, the parallel reference experiment for only LZ coal pyrolysis in the pure N_2 stream was conducted with the TG/DTG curves included in Figure 3 for reference.

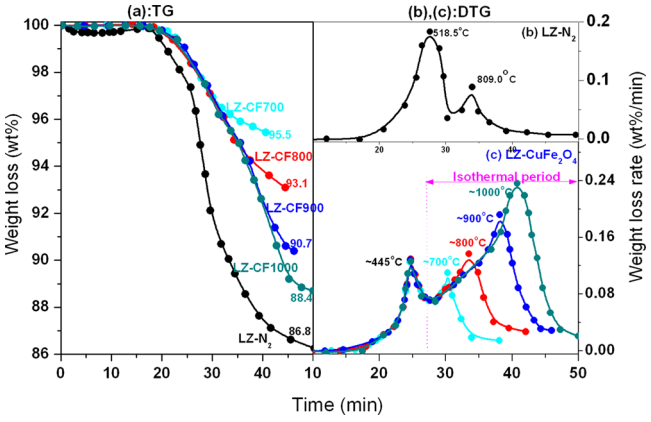

Figure 3. Reaction characteristics of LZ coal with $CuFe_2O_4$ at the different final temperatures: (a) final weight loss (TG), (b) rate of the weight loss for LZ pyrolysis (DTG), and (c) rate of the weight loss between LZ and $CuFe_2O_4$ at the different final temperatures (DTG).

First, the reference experiment for LZ pyrolysis under the N_2 atmosphere was studied. According to the TG/DTG curves for LZ pyrolsyis shown in Figure 3a,b, after elimination of 0.37 wt % of the adsorbed H_2O below 200 °C,[39] two distinct reaction stages occurred sequentially with the two temperatures at the maximal DTG values centering around 518.5 and 809.0 °C, as accompanied by the complex transformation of the LZ coal chemical structure at the first and secondary pyrolysis stages.[40] Furthermore, at the first pyrolysis stage, scission and reuniting of the organic functional groups occurred by emission of a large amount of the oxygenated volatiles such as CO_2, H_2O, CO, and light hydrocarbon gas CH_4,[41] as displayed in Figure 5a below. The maximal rate for the weight loss of LZ at the first pyrolysis stage reached 0.18316 wt%/min. While at the secondary pyrolysis process, disintegration and reorganization of the main carbon matrix resulted[42] with fewer volatile gases emitted. Only a little discernible weight loss rate of 0.08837 wt%/min was obtained, which was in full accordance with the properties of LZ coal.

Then, reaction of LZ coal with $CuFe_2O_4$ at its $\Phi = 1$ was studied with focus on the effect of the final reaction temperature. As displayed in Figure 3a,c, the reaction behavior of LZ coal with $CuFe_2O_4$ differed a lot from LZ pyrolysis. From Figure 3c, for all the four different final temperature cases, the peak temperatures of LZ coal reaction with $CuFe_2O_4$ at the first stage were overlapped and fixed around 445 °C, with the maximal rate of the total weight loss of LZ with $CuFe_2O_4$ reaching 0.12522 wt%/min, which mainly resulted from the atomic oxygen transferred from the $CuFe_2O_4$ and further oxidation of the volatile gases emitted from LZ coal, as validated in Figure 5b (below) by gaseous FTIR analysis. Notably, the first peak temperature for LZ coal reaction with $CuFe_2O_4$ was far lower than those for LZ coal reaction with $MnFe_2O_4$ by 128 °C,[43] $CoFe_2O_4$ by 130 °C,[44] and $NiFe_2O_4$ by ~145 °C[45] under the same reaction condition in our previous research, which fully displayed the higher reactivity of $CuFe_2O_4$ than other ferrite candidates above.

At the second reaction stage, it was noted that the effect of the final reaction temperature on the LZ coal with $CuFe_2O_4$ was quite prominent. A great change in the maximal weight loss rate was observed as shown in Figure 3c. At the lowest final temperature, 700 °C, the second maximal rate of the weight loss for LZ reaction with $CuFe_2O_4$ reached 0.10969 wt%/min, still lower than 0.12522 wt%/min at the first reaction stage. But as the final temperature increased from 700 to 800 °C, the net increase in the maximal rate of the total weight loss reached by 0.02715 wt%/min for the reaction between LZ coal and $CuFe_2O_4$ due to the advantages involved, including the enhanced temperature on the pyrolysis of LZ coal, faster atomic oxygen transfer from $CuFe_2O_4$, and their interaction. When the final temperature was further elevated to 900 °C, relative to the maximal weight loss rate at the final temperature 800 °C, a great net increase in the maximal total weight loss rate occurred, with the net value reaching 0.1936 wt%/min, much higher than those found for reactions of LZ coal with $MnFe_2O_4$ (0.1544 wt%/min),[43] $CoFe_2O_4$ (0.1078 wt%/min),[44] and $NiFe_2O_4$ (0.0874 wt%/min)[45] in our previous research. According to the research above for O_2 emission from $CuFe_2O_4$, such a great increase in the maximal weight loss rate was mainly owe to emission of O_2 through direct decomposition of $CuFe_2O_4$ and its further reaction with the residual char left, as validated in our previous research.[7] Finally, the final reaction temperature was further increased to 1000 °C, the net increase of the maximal weight loss rate for LZ coal reaction with $CuFe_2O_4$ slowed down a little and descended to 0.04456 wt%/min as compared to that value (i.e., 0.05482 wt %/min) at the period between 800 and 900 °C, mainly due to the partial sintering and reactivity deterioration of $CuFe_2O_4$ at the further enhanced temperature 1000 °C, which will be discussed below, though the higher temperature would promote the LZ coal pyrolysis without $CuFe_2O_4$ addition as well as the reaction with $CuFe_2O_4$. Therefore, in the realistic CLC system of coal, $CuFe_2O_4$ was preferred as a good OC, and a proper temperature should be determined to improve the maximal reaction rate of coal with OC and thus to realize operation of the CLC system with lower OC inventory and shorter residence time.[46]

3.3. Conversions of $CuFe_2O_4$ OC Reaction with LZ Coal at Different Temperatures. In order to illuminate the oxygen transfer from $CuFe_2O_4$ and its further contribution to LZ coal at the different reaction temperatures in a realistic CLC system from 700 to 1000 °C, based on the TG data presented in Figure 3 above for LZ coal reaction with $CuFe_2O_4$, two conversions indexes, including the mixture conversion index $X_{LZ\text{-}OC}$ for LZ coal reaction with $CuFe_2O_4$ and OC conversion index X_{OC} for oxygen transfer from the $CuFe_2O_4$, were calculated using eqs 1−4. The results attained are displayed in Figure 4.

In Figure 4a for the reaction of LZ coal with $CuFe_2O_4$ at the final reaction temperature 700 °C, according to the $CuFe_2O_4$ oxygen-transfer mechanisms investigated above, only atomic oxygen in the $CuFe_2O_4$ is transferred and further reacted with the gaseous products evolved from LZ pyrolysis. Therefore, the

DOI: 10.1021/acs.energyfuels.6b02525
Energy Fuels 2017, 31, 5233−5245

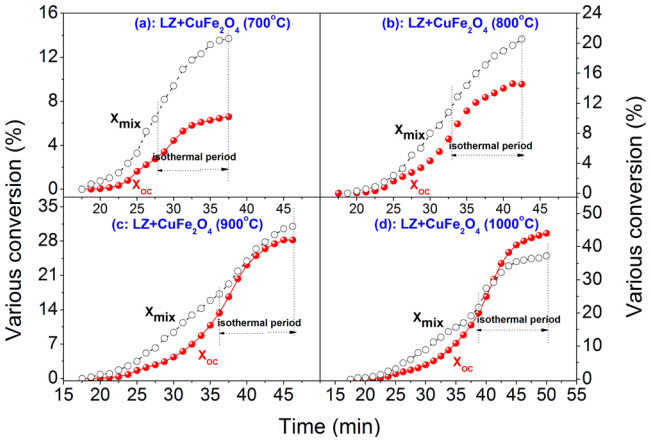

Figure 4. Conversions for LZ coal reaction with $CuFe_2O_4$ OC at the different final temperatures from 700 to 1000 °C.

mixture conversion index $X_{LZ\text{-}OC}$ is always higher than that of the OC conversion index X_{OC}. Especially after the 700 °C isothermal period, the $X_{LZ\text{-}OC}$ reached 14.74%, much higher than that of X_{OC} as 6.59% with the difference reaching 8.15%. As the final temperature increased to 800 °C, as indicated in Figure 4b, though the total conversion index $X_{LZ\text{-}OC}$ is still higher than X_{OC} during the whole reaction stage, after the 800 °C isothermal period, the difference between the $X_{LZ\text{-}OC}$ (21.98%) and $X_{LZ\text{-}OC}$ (14.56%) decreased to 7.42%, mainly because the higher temperature more favored the atomic oxygen transfer from the $CuFe_2O_4$ than that of LZ coal devolatilization and its further oxidation by $CuFe_2O_4$ OC. Furthermore, as the final temperature increased to 900 °C, from Figure 4c, it could be found that a great change occurred with both the mixture conversion index $X_{LZ\text{-}OC}$ and OC conversion index X_{OC} increasing. Especially after the 900 °C isothermal period, according to the $CuFe_2O_4$ oxygen-transfer mechanisms studied above, because the O_2 emission and direct combustion of the pyrolysis residues of LZ dominated, the X_{OC} quickly increased to 28.20%, much approaching the mixture conversion index $X_{LZ\text{-}OC}$ as 30.99%, and thus the oxygen provided from $CuFe_2O_4$ nearly matched the oxygen needed to oxidize LZ coal. Finally, when the final reaction temperature increased to 1000 °C, as shown in Figure 4d, it could be found that during the 1000 °C isothermal period, the OC conversion index X_{OC} quickly increased to 44.02%, much higher than the mixture conversion index as 37.69%, which implied that the oxygen provided from the $CuFe_2O_4$ more than that the oxygen needed for LZ coal oxidation.

Overall, through the two defined conversion indexes, the pyrolysis/gasification of LZ coal, OC transfer from OC, and their further reaction could be quantitatively evaluated, which not only elucidated whether the oxygen provided from OC matched the oxygen needed for LZ coal oxidation, but also had great implications to further determine the optimized reaction conditions for sufficient utilization of LZ coal in CLC.

3.4. Gaseous Reaction Products of LZ Coal wih $CuFe_2O_4$ OC by FTIR Analysis. Gases emitted from the TG was continuously introduced to the gas cell of the coupled FTIR spectrometer and further in situ analyzed to fully understand the thermal conversion behavior of the LZ coal for its reaction with $CuFe_2O_4$. The gaseous FTIR spectra related to the pyrolysis of LZ coal in the pure N_2 stream and their reaction with $CuFe_2O_4$ at the final temperature 900 °C are taken as an example and presented in Figure 5.

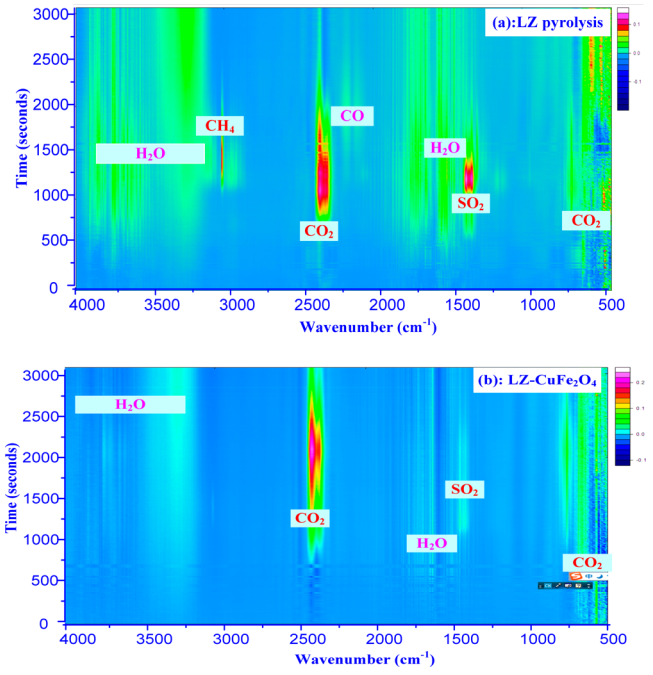

Figure 5. Gaseous FTIR spectra at the final temperature 900 °C: (a) LZ pyrolysis under N_2 and (b) LZ reaction with $CuFe_2O_4$.

As to the pyrolysis process of LZ coal in the pure N_2 stream as a reference, in Figure 5a, the gaseous products evolved as functions of both the wavenumber in the X axis and the time or temperature (as referenced to the Figure 3 above) in the Y axis are presented. Meanwhile, based on the linear relationship between the IR absorbance intensity and the gas concentration,[47] the IR absorbance intensity bar with different colors was provided in the upper righthand of this figure and could be used to indicate the relative concentrations of the evolved gaseous products. From Figure 5a, the main volatiles for LZ pyrolysis in the N_2 atmosphere were identified as such oxygenated gaseous components as H_2O, CO_2, CO, and some light aliphatic gases such as CH_4, which mainly evolved from different organic functional groups of different thermal stabilities involved in LZ coal,[48,49] as analyzed in more detail below. First, H_2O was observed to occur with two broad IR representative wavenumber regions around 3900−3500 cm^{-1} and the accompanied region around 1600 cm^{-1}, and even not to terminate after LZ pyrolysis at the final temperature 900 °C. Different sources of the formed H_2O during the whole period for LZ pyrolysis were analyzed[50] and mainly resulted from emission of a little H_2O adsorbed in the original LZ coal sample below ∼200 °C, liberation of prolific H_2O through some chemically bound water in various minerals[49] and decomposition of different oxygen-containing groups of low thermal stability (e.g., phenolic −OH groups) in LZ coal[51] until 650 °C. Above 650 °C, release of H_2O was still observed and mainly resulted from disintegration of the oxygen-containing groups of higher thermal stability in LZ coal. While for CO_2, it was identified by the IR characteristic wavenumber region 2240−2402 cm^{-1}, and most of CO_2 was produced around 400−550 °C in this research through cracking and reforming of the carboxyl functional groups present in LZ coal.[52] Then, some

DOI: 10.1021/acs.energyfuels.6b02525
Energy Fuels 2017, 31, 5233−5245

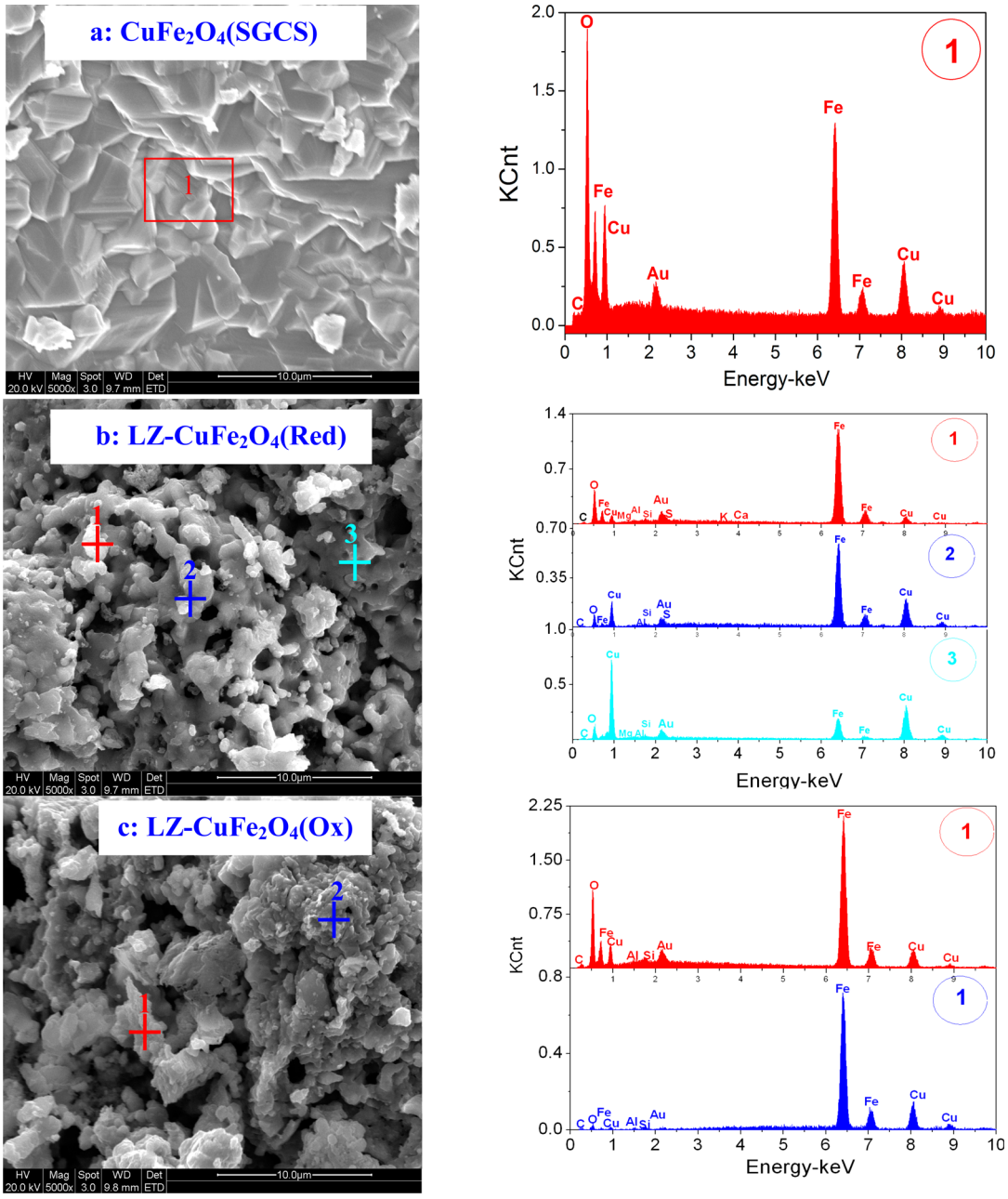

Figure 6. FSEM-EDX analysis: (a) SGCS-prepared $CuFe_2O_4$, (b) solid reaction product of LZ with $CuFe_2O_4$ at the final temperature 900 °C (Φ = 1), and (c) solid oxidation products of the reduced $CuFe_2O_4$ with air.

light hydrocarbon gases were produced at the absorbance region of 2850−3200 cm^{-1}, of which CH_4 was dominated with its maximal concentration around 510 °C, mainly resulting from scission of the methyl groups.[42] Subsequent to H_2O, CO_2, and CH_4, a small amount of CO at the IR characteristic wavenumber 2180 cm^{-1} was observed to form above 500 °C and mainly resulted from rupture of various C═O functional groups with the high thermal stability. CO was reported to be temperature dependent with its yield generally increasing with the reaction temperature,[48] and in this research CO yield was found to mainly increase between 500 and 700 °C. As to H_2, its production was reported to occur over 700 °C through condensation of the aromatic structures[53]and increase with temperature,[50] but it could not be detected in Figure 5a due to its inactivity to FTIR.[49]

Different from H_2O, CO_2, CH_4, and CO, as mentioned above for the LZ coal pyrolysis under the pure N_2 atmosphere, SO_2 emitted from LZ pyrolysis under N_2 was also produced at the IR wavenumber 1450−1300 cm^{-1} with an accompanied IR peak around 1150 cm^{-1},[54] which was inferred to mainly result from the inorganic sulfur minerals in LZ coal,[55,56] instead of from the contribution of various organic functional groups. Apart from SO_2, H_2S was generally dominated among all the potential sulfur gases during pyrolysis of coal,[57] but H_2S could not be identified by FTIR analysis due to its weak IR absorbance.[49]

But for LZ coal reaction with $CuFe_2O_4$, from the FTIR spectrum of the gaseous products evolved as depicted in Figure 5b, the main gaseous products determined were CO_2, H_2O, and a little SO_2. The concentrations of CO and CH_4 emitted from

DOI: 10.1021/acs.energyfuels.6b02525
Energy Fuels 2017, 31, 5233−5245

Table 2. Relative Atomic Concentration of the Elemental Compositions[a]

sample		atomic concentration (at.%) C	O	Fe	Cu	Si	Al	S	K	Ca	Mg
$CuFe_2O_4$ (SGCS)		0.12	57.23	28.38	14.27	N.A.	N.A.	N.A.	N.A.	N.A.	N.A.
LZ + $CuFe_2O_4$ (red.)	spot 1	9.81	44.71	30.59	5.77	1.61	1.60	0.90	0.56	0.48	1.25
	spot 2	8.95	35.78	24.63	27.04	0.90	0.64	0.49	0.45	0.55	0.15
	spot 3	8.13	24.98	15.26	46.92	1.39	1.14	0.16	0.41	0.43	1.07
LZ + $CuFe_2O_4$ (ox.)	spot 1	0.22	48.52	30.62	18.10	0.77	0.66	0.09	0.23	0.28	0.49
	spot 2	0.15	38.20	36.53	22.32	1.03	0.81	0.08	0.19	0.18	0.42

[a]N.A. means not available.

LZ coal were quite low and not identifiable in Figure 5b, though complete elimination of these combustible gases to realize the full conversion of coal was not easy during LZ coal reaction with $CuFe_2O_4$. Among all the gaseous products presented in Figure 5b for LZ coal reaction with $CuFe_2O_4$, CO_2 was of the largest and formed through both reaction of $CuFe_2O_4$ with the carbonaceous gases at the first and secondary pyrolysis stage of LZ coal, and the direct combustion of the residual char with the O_2 emitted from $CuFe_2O_4$. In addition, though direct reaction of the residual char with $CuFe_2O_4$ was also possible by their effective contact in the TGA, as observed by Siriwardane et al.,[58] such reaction could not be initiated in the more realistic CLC system using the fluidized bed reactor. As to SO_2, from Figure 5b, it was observed as the only discernible gaseous sulfur component during the reaction between LZ coal of high sulfur content with $CuFe_2O_4$ at 450 °C, which was formed through reactions of $CuFe_2O_4$ with the gaseous sulfur species evolving from LZ coal.[28]

3.5. Solid Products of LZ Coal with $CuFe_2O_4$ Analyzed by FSEM-EDX and XRD. After the previous research on the reaction behavior of LZ coal with $CuFe_2O_4$ by TGA-FTIR, in order to further illuminate the oxygen transfer from $CuFe_2O_4$ and its interaction with LZ coal, morphologies and distribution of the elements of interest for the solid reaction products from LZ coal with $CuFe_2O_4$ at the final temperature 900 °C at $\Phi = 1$ and further oxidization of the reduced $CuFe_2O_4$ with air at the same final temperature were further analyzed with field emission scanning electron microscopy coupled with energy-dispersive X-ray spectroscopy (FSEM-EDX) and presented in Figure 6b,c, respectively. Meanwhile, based on the EDX data, the elemental compositions involved in the solid products were quantified using the standard correction method by combination of atomic number correction (Z), absorption correction (A), and fluorescence correction (F),[59] as listed in Table 2. Furthermore, in Figure 7, crystalline phases involved in the solid product of the reduced $CuFe_2O_4$ by LZ coal and then reoxidization with air were identified using XRD analysis.

First, from the SEM image of the prepared $CuFe_2O_4$ using SGCS method as displayed in Figure 6a, even calcined under the air atmosphere at 950 °C for 2 h, it still presented as polyhedral appearance with sharp edges, fully indicating its good resistance to sintering. Through the EDX analysis of the atomic distributions of Cu, Fe, and O, it could be determined that the desired $CuFe_2O_4$ was formed, in consistence with the XRD analysis in Figure 1c. But different from the prepared $CuFe_2O_4$, from Figure 6b for the reaction of the prepared $CuFe_2O_4$ with LZ coal, a little sintering occurring for the reduced Cu on the uppermost surface was observed through fusion and coalescence of the reduced Cu grains, though pores

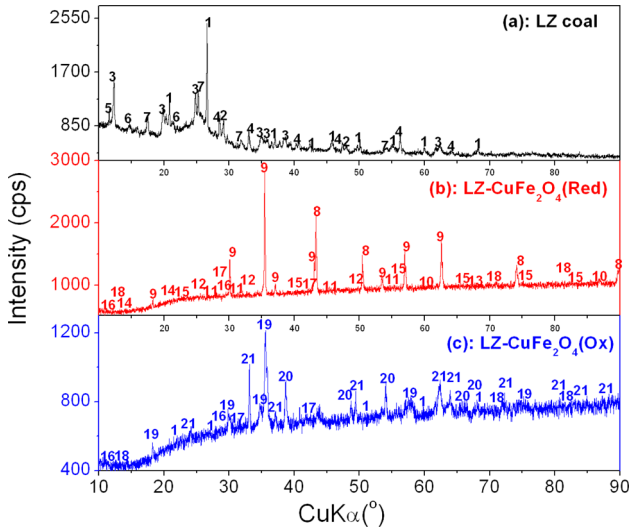

Figure 7. XRD analysis: (a) LZ raw coal, (b) solid products for LZ coal with $CuFe_2O_4$ OC at the final temperature 900 °C ($\Phi = 1$), and (c) solid oxidation products of the reduced $CuFe_2O_4$ with air. Peak identification in this figure: 1, quartz (SiO_2); 2, calcite ($CaCO_3$); 3, kaolinite ($Al_2Si_2O_5(OH)_4$); 4, pyrite (FeS_2); 5, gypsum ($CaSO_4 \cdot 2H_2O$); 6, iron sulfate ($Fe_2(SO_4)_3$); 7, illite ($KAl_2(Si_3Al)O_{10}(OH)_2$); 8, copper; 9, magnitite (Fe_3O_4); 10, iron sulfide (FeS); 11, copper sulfide (Cu_2S); 12, ferrosite ($FeSiO_3$); 13, fayalite (Fe_2SiO_4); 14, silimanite (Al_2SiO_5); 15, gehlenite ($Ca_2Al_2SiO_7$); 16, wollastonite ($CaSiO_3$); 17, anorthite ($CaAl_2Si_2O_8$); 18, potassium-feldspar ($KAlSi_3O_8$); 19, copper ferrite ($CuFe_2O_4$); 20, copper oxide (CuO); 21, hematite (Fe_2O_3).

of different sizes were still existent. Furthermore, from Table 2, based on the selected three spots across the SEM picture shown in Figure 6b for the solid product of LZ coal with $CuFe_2O_4$, the atomic distributions of Cu, Fe, and O in the three spots were found greatly heterogeneous and quite different from our previous similar research on the reaction of $CuFe_2O_4$ with several other coals with lower ash contents,[7] though the main reduced counterparts of $CuFe_2O_4$ were the same and identified as Cu and Fe_3O_4 by XRD analysis shown in Figure 7b.

Furthermore, from the bottom spot 1 to the spot 3 at the uppermost level shown in Figure 6b for LZ coal reaction with $CuFe_2O_4$, both atomic fractions of Fe and O decreased from 30.59% and 44.71% on the spot 1 to 15.26% and 24.98% on the spot 3, respectively, while the atomic of Cu increased a lot from 5.77% on the spot 1 to 46.92% on the upper spot 3, which could result in the segregation of Cu and Fe_3O_4. Such uneven distributions of Cu, Fe, and O were complex due to different reasons as analyzed in more detail below. As to Cu, its uneven

DOI: 10.1021/acs.energyfuels.6b02525
Energy Fuels 2017, 31, 5233−5245

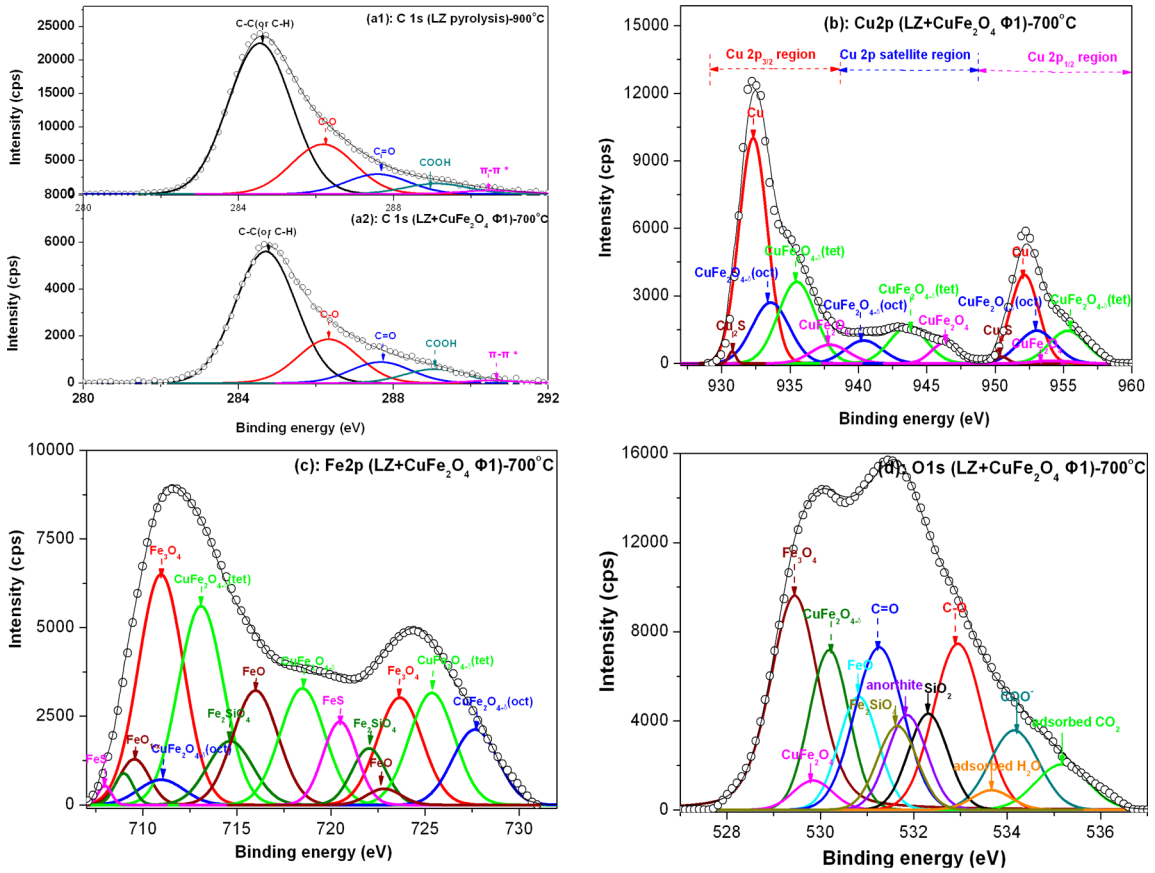

Figure 8. XPS spectra of LZ coal reaction with $CuFe_2O_4$ at the final temperature 700 °C (Φ = 1): (a) C 1s spectra for the solid products of both LZ pyrolysis (a1) and reaction with $CuFe_2O_4$ (a2), (b) Cu 2p spectra, (c)Fe 2p spectra, and (d) O 1s spectra.

distribution was mostly attributed to the easy mobility of the reduced Cu grains for its low melting pointing (~1085 °C) as observed in our previous research[8] and its affinity to H_2S emitted from LZ coal by reaction of Cu with H_2S ($Cu + H_2S \rightarrow Cu_2S + H_2$).[60] As to Fe, its uneven distribution was possibly due to interaction of the deeply reduced FeO with SiO_2 involved in LZ coal through reaction of FeO with SiO_2 to form Fe_2SiO_4 (i.e., $2FeO + SiO_2 \rightarrow Fe_2SiO_4$).[61] As to O, besides the reaction of the reduced $CuFe_2O_4$ with the minerals in LZ coal, interaction of the minerals involved in LZ coal should be also considered. As shown in Figure 7a, the main minerals involved the LZ original coal were identified by XRD analysis as quartz (SiO_2), kaolinite ($Al_2Si_2O_5(OH)_4$), illite ($KAl_2(Si_3Al)O_{10}(OH)_2$)), and calcite ($CaCO_3$). But after the reaction of LZ coal and $CuFe_2O_4$ at 900 °C, as indicated in Figure 7b, the main minerals changed a lot, and such silicates as silimanite (Al_2SiO_5), gehlenite ($Ca_2Al_2SiO_7$), anorthite ($CaAl_2Si_2O_8$), and potassium-feldspar ($KAlSi_3O_8$) were formed, which made the O atomic distribution much uneven.

Finally, good regeneration of the reduced OC is also very important. Further oxidation of the reduced $CuFe_2O_4$ with air was studied. The SEM pattern of the regenerated $CuFe_2O_4$ is presented in Figure 6c. Different from LZ coal reaction with $CuFe_2O_4$ above, the re-oxidized solid products were still porous without agglomeration and sintering occurring, mainly due to the higher melting points of the oxidized products formed, including CuO, Fe_2O_3, and $CuFe_2O_4$, as validated in Figure 7c for XRD analysis. But complete regeneration of the reduced $CuFe_2O_4$ to its original form was not reached. Besides the formed $CuFe_2O_4$ as desired, some separate CuO and Fe_2O_3 were also formed, which did not further combine each other to form $CuFe_2O_4$ again due to the uneven distribution of the reduced Cu and Fe species during the reduction of $CuFe_2O_4$ with LZ coal, as observed above. Therefore, evolution and interaction of the mineral involved in LZ coal with the reduced $CuFe_2O_4$ were much complex, and deeper research would be further conducted in a more realistic CLC system of coal.

3.6. Investigation of the Solid Reaction Products of $CuFe_2O_4$ OC with LZ Coal by XPS. The reactions involved in the coal-fuelled CLC are of typical gas−solid reactions accompanied by the pyrolysis of coal, gasification of the residual char, and their further reactions with OC simultaneously, which made deep understanding of coal reaction with OC during the CLC process difficult. In order to further reveal the variation of the LZ coal chemical structure in its reaction process of LZ coal with $CuFe_2O_4$, XPS was adopted as a sensitive surface technique to obtain a mechanistic insight into coal conversion and interaction with $CuFe_2O_4$ at the molecular scale.

3.6.1. Evolution of the Main Carbon Functional Groups in LZ Coal. Sufficient conversion of the carbon species involved in the original coal is critical to efficient CO_2 capture during the CLC process. Therefore, the solid reaction product of LZ coal with $CuFe_2O_4$ at 700 °C was first investigated as a baseline via XPS analysis, though such a temperature is much low in the real CLC system of coal. In order to acquire the main carbon functional groups distributed in the LZ coal and their further evolution in the reaction process with $CuFe_2O_4$, based on the well-defined assigments of the different C 1s binding energy (BE) values and the main carbon-containing groups in coal,[62,63]

DOI: 10.1021/acs.energyfuels.6b02525
Energy Fuels 2017, 31, 5233−5245

i.e., aromatic and aliphatic carbon (C−C/C−H) at 284.6 eV, ether, phenol or alcohol groups (C−O) at 286.3 eV, carbonyl (C═O) at 287.5 eV, carboxylic groups (COOH) at 289.0 eV, carbonate (CO_3^{2-}) at 290.5 eV, and $\pi-\pi^*$ shakeup peak at 291.5 eV due to the aromatic carbon matrix involved in coal,[64] the C 1s XPS profile obtained in the region 280−295 eV was further deconvoluted and provided in Figure 8a. The relative atomic concentrations of the curve-fitted carbon components were quantified by their respective integrated areas as listed in Table 3. In addition, carbon functional groups and their relative

Table 3. Relative Content of the Carbon Functional Groups

	relative content (%)					
sample	C−C/C−H	C−O	C═O	O═C−O	CO_3^{2-}	$\pi-\pi^*$
LZ coal[a]	71.23	11.90	11.60	1.41	3.60	0.27
LZ pyrolysis, 900 °C	64.45	21.24	8.44	4.46	0	1.43
LZ + $CuFe_2O_4$ (red.), 700 °C	62.11	20.64	9.84	6.53	0	0.86

[a]As reported in our previous research.[29]

contents in the LZ solid pyrolysate at the final temperature 900 °C without $CuFe_2O_4$ addition were included as well for comparison.

From Figure 8a1 and Table 3 for the different deconvoluted carbon functional groups and their relative contents of the LZ coal and the solid pyrolysate as collected, it could be observed that relative to the LZ original coal, the relative contents of the different carbon functional groups involved in the solid pyrolysis residue of LZ coal changed greatly. The relative content of the aromatic and aliphatic carbon groups reduced much from 71.23% in the initial LZ coal to 64.45% in its solid pyrolysate due to cracking of the aromatic and aliphatic carbon functional groups (C−C/C−H) of LZ coal during its pyrolysis.[65] Similar to the aromatic and aliphatic carbon functional groups in the pyrolyzed LZ coal, the relative contents of C═O groups decreased along with CO emission.[52,66] On the contrary, the relative contents of C−O groups after LZ pyrolysis was found out to increase from 11.9% to 21.24%, mainly due to their formation through both elimination of the hydroxyl groups[65] as well as the breakage of C═O groups.[67] Meanwhile, after LZ pyrolysis, more COOH groups were formed through the further conversion of the formed C−O groups,[68,69] though COOH groups were reported as thermally unstable[70] and easily decomposed through decarboxylation reaction to form H_2O and CO_2, as discussed in Section 3.4 above.

However, after the reaction of LZ coal and $CuFe_2O_4$ at the final temperature 700 °C, it could be observed from Figure 8a2 and Table 3 that, a great decline of C−C/C−H groups occurred by incorporating more atomic oxygen present in $CuFe_2O_4$ into the C−C/C−H groups. Its relative content decreased to 62.11%, even lower than those present in the pyrolyzed coal at the higher temperature 900 °C, which meant that relative to only pyrolysis of LZ coal at high temperature, introduction of $CuFe_2O_4$ OC was more effective to promote the utilization of C−C/C−H functional groups in the LZ coal. With the decrease of aromatic and aliphatic carbon functional groups of LZ coal, the C−O group content was raised from 11.9% in the initial LZ coal to 20.64% because the C−C/C−H functional groups in the LZ coal was preferentially oxidized.[65] But a little decrease of the relative C═O functional groups was seen, mainly attributable to the competing reactions involved for oxidization of the C−O groups to form the C═O groups[71] and further disintegration of the formed C═O groups through decarbonylation to emit CO.[52] As to the COOH group, a great increase in its relative content was observed to form through further oxidation of the formed C−O functional groups[25] after the reaction between LZ coal and $CuFe_2O_4$.

3.6.2. Distribution of the Reduced $CuFe_2O_4$ OC. In order to better understand the oxygen transfer from $CuFe_2O_4$ OC to the LZ coal and their complex interaction, we identified both the reduced Cu and Fe compounds as well as the O species left in the solid product after reaction of LZ coal with $CuFe_2O_4$ using XPS and presented in Figure 8b−d, respectively.

After the reaction between $CuFe_2O_4$ OC and LZ coal at 700 °C, the collected solid products were analyzed using XPS. From Figure 8b,c, the main Cu species was identified as elemental Cu by its BE value and the corresponding assignment,[72] while the formed Fe species was Fe_3O_4,[73] which was consistent with the XRD bulk analysis in Figure 7b above. Besides these two reduced counterparts, the oxygen-deficient $CuFe_2O_{4-\delta}$ ($0 \le \delta \le 2$)[74] was also formed through partial disintegration of the spinel structure of the prepared $CuFe_2O_4$, where it was found that Cu^{2+} and Fe^{3+} ions in the $CuFe_2O_4$ preferentially took up the octahedral sites of the $CuFe_2O_4$ spinel, which was advantageous for the fast transference of the atomic oxygen to LZ coal for its better oxidization.[36] Meanwhile, on the surface of the solid product for LZ coal reaction with $CuFe_2O_4$ OC, the reduced $CuFe_2O_4$ species was more complex. Besides Cu, Fe_3O_4, and deficient $CuFe_2O_{4-\delta}$, deep reduction of Fe_3O_4 also occurred with a little FeO formed,[75] though FeO was not desired in the realistic CLC process due to the low melting point as well as weak resistance to sintering. In addition, a little Cu_2S[76] was also found to form through interaction of the reduced Cu and H_2S emitted from LZ coal, while Fe_2SiO_4[77] was formed through the interaction between the reduced FeO and SiO_2 involved in LZ coal. As to the $CuFe_2O_4$ observed,[78] it should be formed through re-oxidization during sample transfer for XPS analysis.[60]

Meanwhile, the oxygen species left after the reaction of $CuFe_2O_4$ and LZ coal were very complicated and analyzed by XPS. The O 1s XPS envelope was deconvoluted and provided in Figure 8d. Except for the three organic oxygen-containing groups involved in the LZ coal, including C−O, C═O, and COOH groups, some reduced $CuFe_2O_4$ compounds were also formed, including Fe_3O_4, oxygen-deficient $CuFe_2O_{4-\delta}$, and FeO, as analyzed above. Meanwhile, some silicon-based minerals evolved from LZ coal were also observed, e.g., Fe_2SiO_4, anorthite ($CaAl_2Si_2O_8$), and SiO_2 of different crystallines, far different from those existing in the original LZ coal as referenced in Figure 7a. In addition, some adsorbed H_2O[79] and CO_2[80] were also found due to the high concentration of CO_2 and H_2O formed from LZ coal reaction with $CuFe_2O_4$.

3.6.3. Effect of the Reaction Temperature on the Carbon Functional Groups of LZ Coal. Finally, temperature was considered as one of the important factors in CLC, and its effect on the coal conversion has been widely investigated. Therefore, evolution of the four main carbon-containing groups in the LZ coal was studied during its reaction with $CuFe_2O_4$ at 700, 800, 900, and 1000 °C, as displayed in Figure 9.

From Figure 9 for the reaction of LZ coal with $CuFe_2O_4$ at $\Phi = 1$, the reaction temperature was found most prominent to the aromatic and aliphatic carbon groups in the LZ coal. Especially

DOI: 10.1021/acs.energyfuels.6b02525
Energy Fuels 2017, 31, 5233−5245

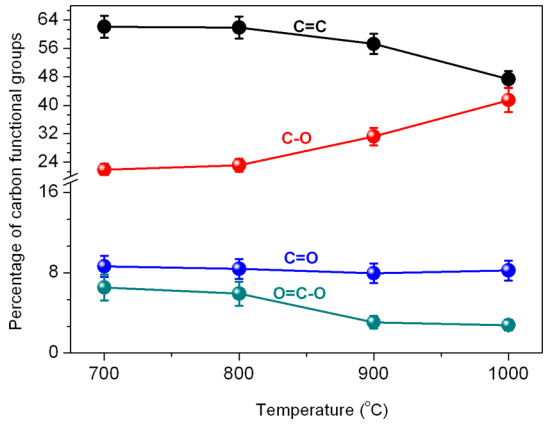

Figure 9. Variation of the main carbon functional groups involved in the LZ coal after being oxidized with $CuFe_2O_4$ OC (Φ = 1) at the different final temperatures.

above 800 °C, due to the O_2 emitted through direct decomposition of $CuFe_2O_4$ and further oxidization of the rest char after the reaction of LZ coal and $CuFe_2O_4$ as disccused above, the relative content of the aromatic and aliphatic carbon groups in LZ fell drastically from 61.91% at 800 °C to 57.26% at 900 °C and further down to 47.33% at 1000 °C, indicating that reaction temperature was one of the effective factors to be considered in CLC for coal conversion. It should be noted that, although the final temperature was raised to 1000 °C in this research, a little higher than the common temperature adopted in realistic CLC coal systems of around 850−950 °C, complete consumption of the C−C/C−H groups in LZ was still not realized. Thefore, besides proper increase of reaction temperature, other measures such as activation of the original coal to promote the efficient utilization of the aromatic and aliphatic carbon groups should be also considered in the future.

Furthermore, with the reduction in the C−C/C−H groups by their oxidization with $CuFe_2O_4$, more C−O functional groups were produced, with the relative content increasing from 21.8% at 700 °C to 41.47% at 1000 °C. But the relative content of COOH groups decreased much from 6.53% at 700 °C to 2.79% at 1000 °C, though still higher than that involved in the original LZ coal as only 1.41%, mainly due to the relatively low thermal stability of COOH groups as pointed out above. While for C═O groups, their relative content was always stabilized around 8% throughout all the different final temperatures, mainly due to the balance between the formed C═O groups via oxidization of the involved C−O groups and the competitive disintegration of the formed C═O groups with CO emission, as discussed above.

Overall, through investigation of the oxygen-transfer mechanisms of $CuFe_2O_4$ and the following reaction of $CuFe_2O_4$ with the typical LZ bituminous coal at the different temperatures through TG analysis, and characterization of the solid reaction products between LZ coal and $CuFe_2O_4$ by FESEM-EDX, XRD, and XPS, more insightful knowledge was obtained for efficient utilization of coal in the realistic coal CLC system.

4. CONCLUSIONS

Reaction temperature is one of the important factors to be considered in a CLC system. Its effect on the reaction of the typical LZ bituminous coal and $CuFe_2O_4$ combined OC was systematically investigated and the following conclusions were reached.

(1) H_2-TPR investigation of the $CuFe_2O_4$ indicated that the first reduction of the Cu^{2+} ion involved in the $CuFe_2O_4$ was beneficial to further reduction of the Fe^{3+} by fast transfer of the atomic oxygen involved, while the TPD investigation indicated that $CuFe_2O_4$ owned the potential to emit O_2 by its direct decomposition with sufficient O_2 emission capacity.

(2) TGA-FTIR analysis of the reaction between $CuFe_2O_4$ and LZ coal showed the better reactivity of $CuFe_2O_4$ for its lower characteristic reaction temperatures at the first stage and higher maximal weight loss rate at the second stage than other ferrite OCs.

(3) Comparison of the two defined conversion indexes at 900 °C indicated that the OC conversion index X_{OC} approached the mixture conversion index $X_{LZ\text{-}OC}$, and thus the oxygen provided from $CuFe_2O_4$ basically matched the oxygen needed for LZ coal oxidation.

(4) Comprehensive investigation of the reaction products of $CuFe_2O_4$ with LZ coal by FESEM-EDX, XRD, and XPS indicated that the $CuFe_2O_4$ was mainly reduced to Cu and Fe_3O_4, and meanwhile some oxygen-deficient $CuFe_2O_{4-\delta}$ was formed, which benefited the oxygen transfer from its octahedral sites.

(5) Through XPS analysis of the carbon functional groups involved in the LZ coal indicated that the limiting factor for efficient utilization of coal during its reaction with $CuFe_2O_4$ was disintegration and conversion of C−C/C−H groups involved at the molecular level, and their utilization degree could be improved with proper increase of the reaction temperature as well as sufficient $CuFe_2O_4$ addition.

AUTHOR INFORMATION

Corresponding Author

*Tel./Fax: (86)371-69127630. E-mail: david-wn@163.com.

ORCID

Baowen Wang: 0000-0003-1376-3683

Haibo Zhao: 0000-0003-4700-4933

Notes

The authors declare no competing financial interest.

ACKNOWLEDGMENTS

This research is funded by the Chinese National Natural Science Foundation (Nos. 51276210, 50906030, and U1404521), Key R&D Program of Henan Province (Nos. 162102210233 and 142100210459), Innovative Research Team in the Universities of Henan Province (No. 16IRTSTHN017), and Scientific Innovation Talent of Henan Province (No. 154100510011). Financial support received from the China Scholarship Council (No. 201508410060) is also greatly gratefully acknowledged.

REFERENCES

(1) Li, F. X.; Fan, L.-S. Clean coal conversion processes-progress and challenges. *Energy Environ. Sci.* **2008**, *1* (2), 248−267.

(2) Adanez, J.; Abad, A.; Garcia-Labiano, F.; Gayan, P.; de Diego, L. F. Progress in chemical-looping combustion and reforming technologies. *Prog. Energy Combust. Sci.* **2012**, *38* (2), 215−282.

DOI: 10.1021/acs.energyfuels.6b02525
Energy Fuels 2017, 31, 5233−5245

(3) Song, T.; Shen, L. H.; Xiao, J.; Chen, D. Q.; Gu, H. M.; Zhang, S. W. Nitrogen transfer of fuel-N in chemical looping combustion. *Combust. Flame* **2012**, *159* (3), 1286−1295.
(4) Jin, H. G.; Hong, H.; Wang, B. Q.; Han, W.; Lin, R. M. A new principle of synthetic cascade utilization of chemical energy and physical energy. *Sci. China, Ser. E: Technol. Sci.* **2005**, *48* (2), 163−179.
(5) Berguerand, N.; Lyngfelt, A. Design and operation of a 10 kW_{th} chemical-looping combustor for solid fuels - testing with South African coal. *Fuel* **2008**, *87* (12), 2713−2726.
(6) Lyngfelt, A. Chemical-looping combustion of solid fuels- Status of development. *Appl. Energy* **2014**, *113*, 1869−1873.
(7) Wang, B. W.; Yan, R.; Zhao, H. B.; Zheng, Y.; Zheng, C. G. Investigation of chemical looping combustion of coal with $CuFe_2O_4$ oxygen carrier. *Energy Fuels* **2011**, *25* (7), 3344−3354.
(8) Wang, B. W.; Zhao, H. B.; Zheng, Y.; Liu, Z. H.; Zheng, C. G. Chemical Looping combustion of petroleum coke with $CuFe_2O_4$ as oxygen carrier. *Chem. Eng. Technol.* **2013**, *36* (9), 1488−1495.
(9) Bao, J. H.; Li, Z. S.; Cai, N. S. Promoting the reduction reactivity of ilmenite by introducing foreign ions in chemical looping combustion. *Ind. Eng. Chem. Res.* **2013**, *52* (18), 6119−6128.
(10) Ge, H. J.; Shen, L. H.; Gu, H. M.; Jiang, S. X. Effect of co-precipitation and impregnation on K-decorated Fe_2O_3/Al_2O_3 oxygen carrier in chemical looping combustion of bituminous coal. *Chem. Eng. J.* **2015**, *262*, 1065−1076.
(11) Guo, Q. J.; Liu, Y. Z.; Jia, W. H.; Yang, M. M.; Hu, X. D.; Ryu, H.-J. Performance of Ca-based oxygen carriers decorated by K_2CO_3 or Fe_2O_3 for coal chemical looping combustion. *Energy Fuels* **2014**, *28* (11), 7053−7060.
(12) Leion, H.; Mattisson, T.; Lyngfelt, A. Solid fuels in chemical-looping combustion. *Int. J. Greenhouse Gas Control* **2008**, *2* (2), 180−193.
(13) Adánez-Rubio, I.; Gayán, P.; Abad, A.; García-Labiano, F.; de Diego, L. F.; Adánez, J. Kinetic analysis of a Cu-based oxygen carrier: relevance of temperature and oxygen partial pressure on reduction and oxidation reactions rates in chemical looping with oxygen uncoupling-(CLOU). *Chem. Eng. J.* **2014**, *256*, 69−84.
(14) Xiao, R.; Song, Q. L.; Zhang, S.; Zheng, W. G.; Yang, Y. C. Pressurized Chemical-looping combustion of Chinese bituminous coal:cyclic performance and characterization of iron ore-based oxygen carrier. *Energy Fuels* **2010**, *24* (2), 1449−1463.
(15) Zhang, S.; Xiao, R.; Zheng, W. G. Comparative study between fluidized-bed and fixed-bed operation modes in pressurized chemical looping combustion of coal. *Appl. Energy* **2014**, *130*, 181−189.
(16) Yang, W. J.; Zhao, H. B.; Ma, J. C.; Mei, D. F.; Zheng, C. G. Copper-decorated hematite as an oxygen carrier for in situ gasification chemical looping combustion of coal. *Energy Fuels* **2014**, *28* (6), 3970−3981.
(17) Dennis, J.; Scott, S. A. In situ gasification of a lignite coal and CO_2 separation using chemical looping with a Cu-based oxygen carrier. *Fuel* **2010**, *89* (7), 1623−1640.
(18) Gayán, P.; Abad, A.; de Diego, L. F.; García-Labiano, F.; Adanez, J. Assessment of technological solutions for improving chemical looping combustion of solid fuels with CO_2 capture. *Chem. Eng. J.* **2013**, *233*, 56−69.
(19) Mattisson, T.; Lyngfelt, A.; Leion, H. Chemical-looping oxygen uncoupling for combustion of solid fuels. *Int. J. Greenhouse Gas Control* **2009**, *3* (1), 11−19.
(20) Liu, Z. Y. Advancement in coal chemistry: structure and reactivity. *Zhongguo Kexue: Huaxue* **2014**, *44* (9), 1431−1438.
(21) Li, Z.-K.; Wei, X.-Y.; Yan, H.-L.; Zong, Z.-M. Insight into the structural features of Zhaotong lignite using multiple techniques. *Fuel* **2015**, *153*, 176−182.
(22) Lin, X. C.; Wang, C. H.; Ideta, K.; Miyawaki, J.; Nishiyama, Y.; Wang, Y. G.; Yoon, S. H.; Mochida, I. Insights into the functional group transformation of a Chinese brown coal during slow pyrolysis by combining various experiments. *Fuel* **2014**, *118*, 257−264.
(23) Wang, J. H.; Du, J.; Chang, L. P.; Xie, K. C. Study on the structure and pyrolysis characteristics of Chinese western coals. *Fuel Process. Technol.* **2010**, *91* (4), 430−433.
(24) Domazetis, G.; Liesegang, J.; James, B. D. Studies of inorganics added to low-rank coals for catalytic gasification. *Fuel Process. Technol.* **2005**, *86* (5), 463−486.
(25) Gong, B.; Pigram, P. J.; Lamb, R. N. Surface studies of low-temperature oxidation of bituminous coal vitrain bands using XPS and SIMS. *Fuel* **1998**, *77* (9-10), 1081−1087.
(26) Zhang, Y. C.; Zhang, J.; Sheng, C. D.; Liu, Y. X.; Zhao, L.; Ding, Q. Z.; Wang, K. Evolution of carbon functionality during coal char combustion in O_2/CO_2 atmosphere. *Proc. Chinese Soc. Electrical Eng.* **2011**, *31* (2), 27−31.
(27) Wang, B. W.; Zheng, Y.; Liu, Z. H.; Zhao, H. B.; Zheng, C. G.; Yan, R. Investigation of chemical looping combustion of coal with Fe_2O_3-based combined oxygen carrier. *Kung Cheng Je Wu Li Hsueh Pao/J. Eng. Thermophys.* **2010**, *31* (8), 1427−1430.
(28) Wang, B. W.; Cao, Y. M.; Li, J.; Wang, W. S.; Zhao, H. B.; Zheng, C. G. Migration and redistribution of sulfur species during chemical looping combustion of coal with $CuFe_2O_4$ combined oxygen carrier. *Energy Fuels* **2016**, *30* (10), 8499−8510.
(29) Wang, B. W.; Wang, W. S.; Ma, Q.; Lu, J.; Zhao, H. B.; Zheng, C. G. In-depth investigation of chemical looping combustion of a Chinese bituminous coal with $CuFe_2O_4$ combined oxygen carrier. *Energy Fuels* **2016**, *30* (3), 2285−2294.
(30) Wang, B. W.; Yan, R.; Lee, D. H.; Zheng, Y.; Zhao, H. B.; Zheng, C. G. Characterization and evaluation of Fe_2O_3/Al_2O_3 oxygen carrier prepared by sol-gel combustion synthesis. *J. Anal. Appl. Pyrolysis* **2011**, *91*, 105−113.
(31) Wang, B. W.; Zhao, H. B.; Zheng, Y.; Liu, Z. H.; Yan, R.; Zheng, C. G. Chemcial looping combustion of a Chinese anthracite with Fe_2O_3-based and CuO-based oxygen carriers. *Fuel Process. Technol.* **2012**, *96*, 104−115.
(32) Shin, H.-C.; Choi, S.-C.; et al. Mechanism of M ferrites (M = Cu and Ni) in the CO_2 decomposition reaction. *Chem. Mater.* **2001**, *13* (4), 1238−1242.
(33) Hosseini, D.; Imtiaz, Q.; Abdala, P. M.; Yoon, S.; Kierzkowska, A. M.; Weidenkaff, A.; Müller, C. R. CuO promoted Mn_2O_3-based materials for solid fuel combustion with inherent CO_2 capture. *J. Mater. Chem. A* **2015**, *3*, 10545−10550.
(34) Gayán, P.; Adánez-Rubio, I.; Abad, A.; de Diego, L. F.; García-Labiano, F.; Adánez, J. Development of Cu-based oxygen carriers for chemical-looping with oxygen uncoupling (CLOU) process. *Fuel* **2012**, *96*, 226−238.
(35) Yu, B.; Zhang, P.; Zhang, L.; Chen, J.; Xu, J. M. Studies on the preparation of active oxygen-deficient copper ferrite and its application for hydrogen production through thermal chemical water splitting. *Sci. China, Ser. B: Chem.* **2008**, *51* (9), 878−886.
(36) Zhang, P.; Yu, B.; Zhang, L. Mechanism of oxygen releasing of copper ferrite in the formation of the corresponding oxygen-deficient compound. *Sci. China, Ser. B: Chem.* **2009**, *52* (1), 101−108.
(37) Kaneko, H.; Yokoyama, T.; Fuse, A.; Ishihara, H.; Hasegawa, N.; Tamaura, Y. Synthesis of new ferrite, Al-Cu ferrite, and its oxygen deficiency for solar H_2 generation from H_2O. *Int. J. Hydrogen Energy* **2006**, *31*, 2256−2265.
(38) Imtiaz, Q.; Hosseini, D.; Muller, C. R. Review of oxygen carriers for chemical looping with oxygen uncoupling (CLOU): Thermodynamics, material development, and synthesis. *Energy Technology* **2013**, *1* (11), 633−647.
(39) Jakab, E.; Till, F.; Várhegyi, G. Thermogravimetric-mass spectrometric study on the low temperature oxidation of coals. *Fuel Process. Technol.* **1991**, *28* (3), 221−238.
(40) Xie, K.-C. *Structure and reactivity of coal: A survey of selected Chinese coals*; Springer-Verlag GmbH: Berlin Heidelberg, 2015; pp 119−178.
(41) Yang, H. P.; Chen, H. P.; Ju, F. D.; Yan, R.; Zhang, S. H. Influence of pressure on coal pyrolysis and char gasification. *Energy Fuels* **2007**, *21* (6), 3165−3170.
(42) Van Heek, K. H.; Hodek, W. Structure and pyrolysis behavior of different coals and relevant model substances. *Fuel* **1994**, *73* (6), 886−896.

DOI: 10.1021/acs.energyfuels.6b02525
Energy Fuels 2017, 31, 5233−5245

(43) Wang, B. W.; Gao, C. C.; Wang, W. S.; Zhao, H. B.; Zheng, C. G. Sulfur evolution in chemical looping combustion of coal with $MnFe_2O_4$ oxygen carrier. *J. Environ. Sci.* **2014**, *26* (5), 1062−1070.
(44) Wang, B. W.; Gao, C. C.; Wang, W. S.; Kong, F. H.; Zheng, C. G. TGA-FTIR investigation of chemical looping combustion by coal with $CoFe_2O_4$ combined oxygen carrier. *J. Anal. Appl. Pyrolysis* **2014**, *105*, 369−378.
(45) Wang, B. W.; Xiao, G.; Song, X. Y.; Zhao, H. B.; Zheng, C. G. Chemical looping combustion of high-sulfur coal with $NiFe_2O_4$-combined oxygen carrier. *J. Therm. Anal. Calorim.* **2014**, *118* (3), 1593−1602.
(46) Mattisson, T.; Lyngfelt, A.; Cho, P. The use of iron oxide as an oxygen carrier in chemical-looping combustion of methane with inherent separation of CO_2. *Fuel* **2001**, *80* (13), 1953−1962.
(47) Eigenmann, F.; Maciejewski, M.; Baiker, A. Quantitative calibration of spectroscopic signals in combined TG-FTIR system. *Thermochim. Acta* **2006**, *440* (1), 81−92.
(48) Xu, W.-C.; Tomita, A. Effect of temperature on the flash pyrolysis of various coals. *Fuel* **1987**, *66* (5), 632−636.
(49) Solomon, P. R.; Serio, M. A.; Carangelo, R. M.; Bassilakis, R.; Gravel, D.; Baillargeon, M.; Baudais, F.; Vail, G. Analysis of the Argonne premium coal samples by thermogravimetric Fourier transform infrared spectroscopy. *Energy Fuels* **1990**, *4* (3), 319−333.
(50) Wang, S. Q.; Tang, Y. G.; Schobert, H. H.; Guo, Y. N.; Gao, W. C.; Lu, X. K. FTIR and simultaneous TG/MS/FTIR study of late permian coals from Southern China. *J. Anal. Appl. Pyrolysis* **2013**, *100*, 75−80.
(51) MacPhee, J. A.; Charland, J.-P.; Giroux, L. Application of TG-FTIR to the determination of organic oxygen and its speciation in the Argonne premium coal samples. *Fuel Process. Technol.* **2006**, *87* (4), 335−341.
(52) Arenillas, A.; Rubiera, F.; Pis, J. J. Simultaneous thermogravimetric-mass spectrometric study on the pyrolysis behavior of different rank coals. *J. Anal. Appl. Pyrolysis* **1999**, *50* (1), 31−46.
(53) Shi, L.; Liu, Q. Y.; Guo, X. J.; Wu, W. Z.; Liu, Z. Y. Pyrolysis behavior and bonding information of coal- A TGA study. *Fuel Process. Technol.* **2013**, *108*, 125−132.
(54) Cheng, H. F.; Liu, Q. F.; Huang, M.; Zhang, S. L.; Frost, R. L. Application of TG-FTIR to study SO_2 evolved during the thermal decomposition of coal-derived pyrite. *Thermochim. Acta* **2013**, *555*, 1−6.
(55) Calkins, W. H. Investigation of organic sulfur-containing structures in coal by flash pyrolysis experiments. *Energy Fuels* **1987**, *1* (1), 59−64.
(56) Szabó, P.; Várhegyi, G.; Till, F.; Székely, T. Investigation of subbituminous coals by thermogravimetry-mass spectrometry: Part 2. Formation of oxygen- and sulphur-containing products. kinetics of the overall mass loss. *Thermochim. Acta* **1990**, *170*, 179−188.
(57) Bassilakis, R.; Zhao, Y.; Solomon, P. R.; Serio, M. A. Sulfur and nitrogen evolution in the Argonne coals: Experiment and modeling. *Energy Fuels* **1993**, *7* (6), 710−720.
(58) Siriwardane, R.; Tian, H. J.; Miller, D.; Richards, G.; Simonyi, T.; Poston, J. Evaluation of reaction mechanism of coal-metal oxide interactions in chemical-looping combustion. *Combust. Flame* **2010**, *157* (11), 2198−2208.
(59) Laskin, A.; Cowin, J. P.; Iedema, M. J. Analysis of individual environmental particles using modern methods of electron microscopy and X-ray microanalysis. *J. Electron Spectrosc. Relat. Phenom.* **2006**, *150* (2−3), 260−274.
(60) Tian, H. J.; Simonyi, T.; Poston, J.; Siriwardane, R. Effect of hydrogen sulfide on chemical looping combustion of coal-derived synthesis gas over bentonite-supported metal-oxide oxygen carriers. *Ind. Eng. Chem. Res.* **2009**, *48* (18), 8418−8430.
(61) Gu, H. M.; Shen, L. H.; Xiao, J.; Zhang, S. W.; Song, T. Chemical looping combustion of biomass/coal with natural iron ore as oxygen carrier in a continuous reactor. *Energy Fuels* **2011**, *25* (1), 446−455.
(62) Pietrzak, R.; Wachowska, H. The influence of oxidation with HNO_3 on the surface composition of high-sulfur coals: XPS study. *Fuel Process. Technol.* **2006**, *87* (11), 1021−1029.
(63) Pietrzak, R.; Grzybek, T.; Wachowska, H. XPS study of pyrite-free coals subjected to different oxidizing agents. *Fuel* **2007**, *86* (16), 2616−2624.
(64) Kelemen, R. K. D.; Kwiatek, P. J.; Rose, K. D. Carbon aromaticity based on XPS π-π^* signal intensity. *Appl. Surf. Sci.* **1993**, *64* (2), 167−174.
(65) Perry, D. L.; Grint, A. Application of XPS to coal characterization. *Fuel* **1983**, *62* (9), 1024−1032.
(66) Hodek, W.; Kirschstein, J.; van Heek, K.-H. Reactions of oxygen containing structure in coal pyrolysis. *Fuel* **1991**, *70* (3), 424−428.
(67) Dong, P. W.; Chen, G.; Zeng, X.; Chu, M.; Gao, S. Q.; Xu, G. W. Evolution of inherent oxygen in solid fuels during pyrolysis. *Energy Fuels* **2015**, *29* (4), 2268−2276.
(68) Chatterjee, K.; Stock, L. M.; Zabransky, R. F. The pathways for thermal decomposition of aryl akkyl ethers during coal pyrolysis. *Fuel* **1989**, *68* (10), 1349−1353.
(69) Vassallo, A. M.; Liu, Y. L.; Pang, L. S. K.; Wilson, M. A. Infrared spectroscopy of coal maceral concentrates at elevated temperature. *Fuel* **1991**, *70* (5), 635−639.
(70) Meldrum, B. J.; Rochester, C. H. Infrared spectra of carbonaceous chars under carbonization and oxidation conditions. *Fuel* **1991**, *70* (1), 57−63.
(71) Clemens, A. H.; Matheson, T. W.; Rogers, D. E. Low temperature oxidation studies of dried New Zealand coals. *Fuel* **1991**, *70* (2), 215−221.
(72) Biesinger, M. C.; Lau, L. W. M.; Gerson, A. R.; Smart, R.St.C. Resolving surface chemical states in XPS analysis of first row transition metals, oxides and hydroxides: Sc, Ti, V, Cu and Zn. *Appl. Surf. Sci.* **2010**, *257* (7), 887−898.
(73) Daou, T. J.; Pourroy, G.; Begin-Colin, S.; Greneche, J. M.; Ulhaq-Bouillet, C.; Legare, P.; Bernhardt, P.; Leuvrey, C.; Rogez, G. Hydrothermal synthesis of monodisperse magnetite nanoparticles. *Chem. Mater.* **2006**, *18* (18), 4399−4404.
(74) Reitz, C.; Suchomski, C.; Haetge, J.; Leichtweiss, T.; Jaglicic, Z.; Djerdj, I.; Brezesinski, T. Soft-templating synthesis of mesoporous magnetic $CuFe_2O_4$ thin films with ordered 3D honeycomb structure and partially inverted nanocrystalline spinel domains. *Chem. Commun.* **2012**, *48* (37), 4471−4473.
(75) Paparazzo, E. On the quantitative XPS analysis of Fe_2O_3 and $Fe_{1-x}O$ oxides. *J. Electron Spectrosc. Relat. Phenom.* **2006**, *154* (1−2), 38−40.
(76) Perry, D. L.; Taylor, J. A. *X*-ray photoelectron and Auger spectroscopic studies of Cu_2S and CuS. *J. Mater. Sci. Lett.* **1986**, *5* (4), 384−386.
(77) Mouayd, A. A.; Koltsov, A.; Sutter, E.; Tribollet, B. Effect of silicon content in steel and oxidation temperature on scale growth and morphology. *Mater. Chem. Phys.* **2014**, *143* (3), 996−1004.
(78) Zhang, Y.; Wei, T. T.; Xu, K. Z.; Ren, Z. Y.; Xiao, L. B.; Song, J. R.; Zhao, F. Q. Catalytic decompostion action of hollow $CuFe_2O_4$ nanospheres on RDX and FOX-7. *RSC Adv.* **2015**, *5* (92), 75630−75635.
(79) Jones, C. F.; LeCount, S.; Smart, R.St.C.; White, T. J. Compositional and structural alteration of pyrrhotite surfaces in solution: XPS and XRD studies. *Appl. Surf. Sci.* **1992**, *55* (1), 65−85.
(80) Pirner, M.; Bauer, R.; Borgmann, D.; Wedler, G. CO_2 adsorption and reaction on polyscrystalline Fe films. *Surf. Sci.* **1987**, *189-190*, 147−160.

DOI: 10.1021/acs.energyfuels.6b02525
Energy Fuels 2017, 31, 5233−5245